Materials Science and Engineering A 391 (2005) 390–401

www.elsevier.com/locate/msea

A kinetic Monte Carlo simulation of film growth by physical vapor deposition on rotating substrates

J. Cho[a,b], S.G. Terry[a], R. LeSar[a,c], C.G. Levi[a,*]

[a] *Materials Department, College of Engineering, University of California, Santa Barbara, CA 93106-5050, USA*
[b] *Department of Mechanical Engineering, State University of New York, Binghamton, NY 13902, USA*
[c] *Theoretical Division, Los Alamos National Laboratory, Los Alamos, NM 87545, USA*

Received 29 December 2003; received in revised form 2 September 2004; accepted 9 September 2004

Abstract

Film growth by physical vapor deposition on rotating substrates is modeled via a kinetic Monte Carlo algorithm on a two-dimensional hexagonal lattice. The motivation is to provide insight on the evolution of porosity during the deposition of thermal barrier coatings (TBCs). The model is implemented on an atomic scale that incorporates the effect of surface diffusion as well as the interplay between surface topography and the changing vapor incidence angle. It is shown that substrate rotation generates voids with a periodicity dependent on the amount of material deposited per revolution. The onset of pore formation and morphology of the pores are linked to the presence of shadowing features on the surface, either in the form of stochastic or crystallographic peaks and valleys evolving during columnar growth, or pre-existing roughness typical of polycrystalline oxide substrates. In addition, various forms of anisotropy develop in the microstructure as a result of the "sunrise–sunset" pattern of vapor incidence characteristic of TBC deposition on, for example, turbine airfoils. Comparison with observations on actual TBCs reveals that the simulations, in spite of their simplicity, capture several key microstructural features characteristic of these complex films.

Keywords: Thermal barrier coatings; Physical vapor deposition; Film growth; Microstructure evolution; Kinetic Monte Carlo

1. Introduction

Electron-beam physical vapor deposition (EB-PVD) is often the technology of choice for the application of thermal barrier coatings (TBCs) on airfoils and other critical components of the gas-turbine engine [1,2]. These coatings are typically based on zirconia partially stabilized with yttria (YSZ) underlaid by a double-layer comprising a thin, thermally grown aluminum oxide (TGO) that provides oxidation/corrosion protection to the substrate, and a metallic "bond coat" that supplies the Al needed to sustain the formation of the TGO [1].

A salient attribute of EB-PVD TBCs is a *segmented* columnar microstructure (Fig. 1) that enables the accommodation of the thermal expansion mismatch with the metallic substrate as the assemblage is thermally cycled during the operation of the engine [3]. Each columnar grain in the microstructure is bonded to the TGO but separated from its neighbors by voided boundaries or "gaps", broadly acknowledged to result from insufficient surface diffusion to overcome "self-shadowing" during deposition [4,5]. The films, however, are typically grown at ∼1000 °C [6], a temperature corresponding to the upper end of zone 2 (∼$0.4T_M$) in the Movchan and Demchishin structure map [7]. The implication is that surface diffusion should be sufficiently active in this range to overcome the effects of atomistic-scale shadowing and the films should be essentially dense. Two factors account for the discrepancy. The first arises from the unique manner in which the airfoils are manipulated over the vapor plume, rotating them about their axis to impart conformal coverage with the desired coating thickness. This produces a "sunrise–sunset" vapor incidence pattern over points on the surface of the airfoil, as schematically illustrated in Fig. 2(a).

* Corresponding author. Tel.: +1 805 893 2381; fax: +1 805 893 8486.
E-mail address: levic@engineering.ucsb.edu (C.G. Levi).

0921-5093/$ – see front matter © 2004 Elsevier B.V. All rights reserved.
doi:10.1016/j.msea.2004.09.015

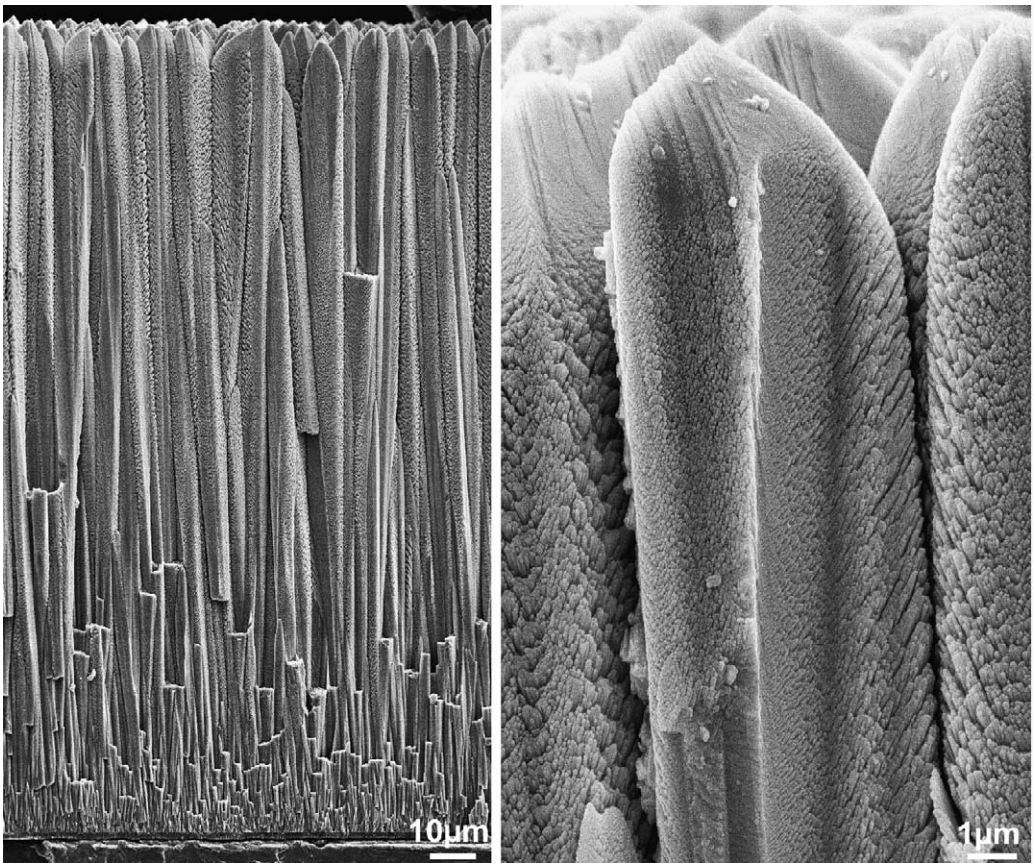

Fig. 1. Typical thermal barrier coating microstructures produced by physical vapor deposition on rotated substrates (images courtesy of J. Yang). Each column is nominally a single crystal, separated from its neighbors by gaps and containing internal porosity with a "feathery" morphology.

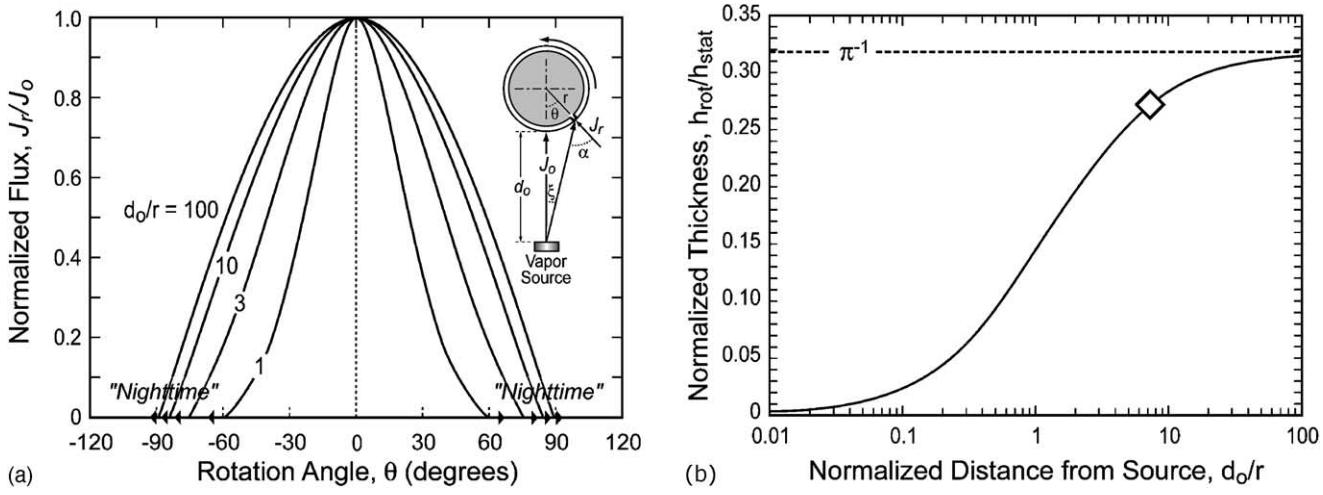

Fig. 2. (a) Instantaneous deposition rate over a differential area on a rotated cylindrical substrate as a function of angular position θ. For each particular geometry, (d_0/r), the deposition rate is null during the "nighttime" part of each rotation cycle and goes through a maximum when the substrate is facing the source and the vapor flux impinges along the surface normal ($\theta = 0$). (b) Ratio of thickness deposited on the rotated substrate per revolution to that deposited on a stationary substrate normal to the plume axis after the same exposure time. Dashed line indicates theoretical maximum of $1/\pi$ and the diamond the point corresponding to the geometry of the evaporator used for parallel experimental studies.

The second factor is the development of considerable roughness as the crystallography of the system dictates that the columns grow with pointed tips, e.g. Fig. 1, rather than forming a flat surface. It is the interplay between this roughness of the growth front and the vapor incidence pattern that exacerbates shadowing and produces inter-columnar porosity under conditions that would normally be expected to yield a dense film [8].

In addition to the inter-columnar gaps, TBCs produced by EB-PVD contain substantial amounts of intra-columnar porosity. In the as-deposited condition, this porosity is typically arranged in a "feathery" morphology, comprising thin ribbon-like pores at an angle to the column axis, e.g. Fig. 1. This "feathery" porosity is beneficial to the insulating properties of the coating [9], albeit potentially detrimental to its erosion resistance. While "feathery" pores typically break down and spheroidize relatively rapidly upon thermal exposure in current TBCs, it has been shown that emerging materials may evolve more slowly, retaining their initially lower conductivity for longer times [10–12].

Understanding the mechanisms leading to the complex pore architecture of thermal barrier coatings, and their dependence on deposition parameters is an essential element in improving their performance and reliability through better design and control of their synthesis. The continuum aspects of these mechanisms are described in a separate publication [13]. Those models, however, focus on geometric effects leading to different scales of shadowing but do not incorporate the effect of surface diffusion. This paper provides an alternate analysis at the atomistic level, wherein surface diffusion effects on the shadowing processes resulting from rotation can be examined more readily.

Background for this work is provided by a number of theoretical methods previously developed to gain a clearer insight into the mechanisms governing the microstructural development in thin films [5,14–21]. Of particular interest are atomic-level computer simulations of the structure and properties based on molecular dynamics (MD), Monte Carlo (MC), and energy-minimization methods [5,14–19,22–24]. A salient feature of the present simulations is the incorporation of both surface diffusion and the peculiar pattern of vapor incidence resulting from rotation of airfoils while being coated by EB-PVD. The study systematically explores variations in process parameters as well as surface characteristics. While the atoms are being deposited at finite temperature, surface morphologies are continuously evolved through successive atomic jumps. Each atom will have a finite probability of jumping, provided that there are available neighboring voids into which it can jump. The system is modeled using the kinetic Monte Carlo (KMC) approach, in which the sequence of configurations generated by MC procedures are related to the time evolution of the system [25–29]. This method can employ relatively large numbers of atoms over long time-scales, in contrast to molecular dynamics simulations that are limited to nanosecond time-scales. The systematic studies undertaken here should be helpful not only in formulating processing/structure relations needed to predict film microstructure, but also in understanding certain observations from experimental work.

2. Simulation methodologies

2.1. Deposition on rotating substrates

The geometric features of different deposition scenarios relevant to thermal barrier coatings have been discussed elsewhere [8,30]. While substrate rotation is typically used to apply a PVD coating to a component of complex geometry, the current model considers for simplicity a cylindrical substrate of unit length. In this scenario, the substrates are rotated about an axis perpendicular to the plume axis, and also to the plane of vapor incidence (Fig. 2(a)). (The plane of vapor incidence is defined as that containing the substrate normal and the line-of-sight direction of the incident atoms.) This rotation has two important implications for the subsequent implementation of the atomic ballistic deposition model. First, the vapor incidence angle of the atoms on the substrate is a function of time, and so is the deposition rate over a differential area of the substrate.

The vapor flux is assumed to have a typical cosine distribution with angle ξ from the plume axis [31] (see Fig. 2). A reference flux, J_0, is defined as that impinging on a planar stationary substrate whose normal is co-linear with the plume axis, placed at a distance d_0 from the source. The deposition rate over a differential area of a cylindrical substrate of radius r whose point of closest approach to the source is also d_0, can be written as a function of the system geometry (d_0/r) and the angular position, θ, in the following form:

$$\frac{J_\mathrm{r}(J_0, d_0/r, \theta)}{J_0} = \frac{(d_0/r)^2[(1+(d_0/r))\cos\theta - 1][(1+d_0/r) - \cos\theta]^m}{[1+(1+d_0/r)^2 - 2(1+d_0/r)\cos\theta]^{(m+3)/2}} \quad (1)$$

where J_r is the instantaneous component of the flux normal to the substrate (thickness per unit time or volume per unit area per unit time) and m the exponent in the "cosine law" (taken as $m = 1$ in the present simulations). The vapor incidence angle, α, is given by

$$\alpha\left(\theta, \frac{d_0}{r}\right) = a\cos\left\{\frac{(1+d_0/r)\cos\theta - 1}{[1+(1+d_0/r)^2 - 2(1+d_0/r)\cos\theta]^{1/2}}\right\} \quad (2)$$

while θ is related to time through ω, the rate of substrate rotation in revolutions per unit time:

$$\frac{\mathrm{d}\theta}{\mathrm{d}t} = 2\pi\omega \quad (3)$$

It is apparent from Fig. 2(a) that during over half of the revolution, the deposition rate over the differential area is zero. This occurs during the "nighttime" portion of each cycle, bounded by θ_{ss} and θ_{sr}, the "sunset" and "sunrise" values of the angular position θ, wherein the vapor flux is tangential to the surface. This results in a reduction in the effective deposition rate on a rotated cylindrical substrate of diameter $2r$ compared with that achieved on a stationary substrate of equivalent width, $2r$, which would have the same projected area normal to the vapor source. The ratio of film thickness deposited on a rotated substrate per revolution, h_{rot}, to the thickness deposited on the equivalent stationary substrate, h_{stat}, in the same time is given by

$$\frac{h_{rot}}{h_{stat}} = \frac{1}{2\pi J_0}\int_{\theta_{sr}}^{\theta_{ss}} J_r\left(J_0, \frac{d_0}{r}, \theta\right) \mathrm{d}\theta \quad (4)$$

The ratio is plotted in Fig. 2(b), which shows it to be an increasing function of d_0/r with an upper asymptote π^{-1}. This limit arises because for $d_0/r \to \infty$ the mass of vapor captured by a stationary substrate of width $2r$ during the time equivalent to one revolution is distributed over the total area of the cylinder, $2\pi r$.[1] Conversely, for a similar set of reference conditions (J_0, d_0/r) the thickness ratio diminishes as $d_0/r \to 0$ because the effective capture area decreases in relation to the area of the cylinder, and so does the exposure time as the tangential velocity increases with r for the same value of ω.

2.2. Atomic ballistic deposition (ABD) model

For simplicity, the problem is approached as one of deposition of atoms, rather than the more complex deposition of the various types of species occurring in the deposition environment of YSZ [32]. A two-dimensional hexagonal lattice model is employed in the simulation of physical vapor deposition (Fig. 3). Sites on the lattice are either occupied or unoccupied by atoms and two atoms are forbidden to share the same site. Surface atoms are those with a coordination number CN ≤ 5. This is done so that re-entrant points in the surface are allowed. A corollary is that internal pore surfaces are also allowed to evolve, and vacancies in the bulk are mobile. However, the activation energy for a vacancy jump in the bulk is sufficiently high relative to other events that its probability is low in the temperature range of interest.

Before the deposition begins, the atoms occupy all substrate sites of the simulation cell ($y = 0$ if substrate is planar), whereas the rest of the lattice is empty. Each atom is dropped from a randomly chosen x position at a height y_0, greatly exceeding that of the surface atoms. The atoms then follow linear trajectories (assuming no collision with gas atoms) in the direction of vapor incidence (varying between -90° and 90° according to a prescribed algorithm, as described below) until they touch the surface. Periodic boundary conditions are imposed in the x-direction while the depositing atoms are traveling. The "touching" condition is satisfied when one of the distances between the dropped atom and its neighbors becomes shorter than an interatomic distance. The vapor incidence angle (VIA), α, is defined as the angle between the surface normal and the direction of vapor incidence.

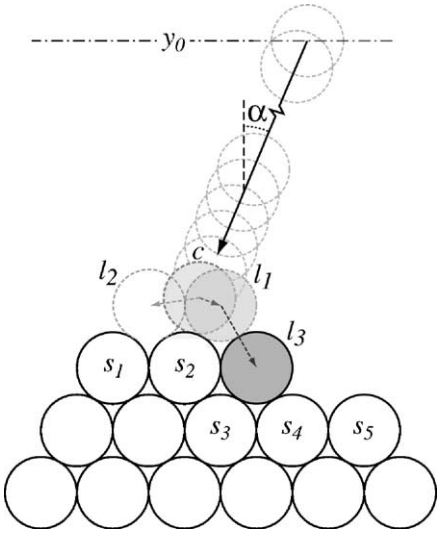

Fig. 3. Schematic diagram to illustrate the events associated with the deposition of an atom in the ABD model. The position of first contact with the surface is denoted by "c" and the available lattice sites into which the atom can move are l_1, l_2, l_3, with coordination numbers of 1, 2 and 3, respectively. The surface atoms, i.e. those with coordination numbers ≤5, are labeled s_i.

All atoms are assumed to stick upon landing and immediately relax to a stable site, defined as one having at least two neighboring atoms, either to the right or left of the impact point in the two-dimensional lattice. Fig. 3 shows a snapshot during deposition to illustrate the mechanism of the aforementioned attachment. As soon as the atom is in contact with one of the surface atoms (position c in Fig. 3), it moves to the closest empty site in the lattice, i.e. position l_1.[2] If the new position was coordinated by at least two atoms, e.g. l_2, the adatom will stop there and any subsequent motion would be governed by the diffusional kinetics of the surface. However, if the closest lattice position was only coordinated by one atom, as is l_1 in Fig. 3, then the adatom will move instantaneously to the next available lattice site with CN ≥ 2 and a lower activation barrier, i.e. l_3 rather than l_2. The assumption is that this initial relaxation process is faster than any other rearrangements that may occur on the surface as a result of

[1] This limit varies depending on the selection of the reference distance for measuring the flux J_0. As shown elsewhere, if the reference stationary substrate was placed normal to the vapor plume axis at a distance equal to that of the rotation axis, the maximum in the ratio J/J_0 would be greater than 1 and π^{-1} would be a lower limit to the normalized deposition rate [30].

[2] It has been suggested that the selection should be biased by the direction of incidence [33], which would make position l_2 more favorable even though the displacement required is longer. However, a criterion of closest available site is adopted here for simplicity.

diffusion, and also occurs in a shorter time than the interval between two adatom arrivals. Once the atom has reached a stable site, other atoms in the surface are allowed to undergo diffusional motion, as described below.

After a time prescribed by the deposition rate, the next atom will be dropped from the same height at a new randomly chosen x location. As the angular position θ is changed in discrete increments according to the prescribed rotation rate (Eq. (3)), the number of atoms deposited during the corresponding time increment and their angle of incidence are determined by Eqs. (1) and (2), respectively.

2.3. Surface diffusion using a kinetic Monte Carlo method

The KMC method is particularly beneficial for systems where events occur on widely varying time scales [34], as in the present situation wherein there are large differences in the activation barriers of various diffusional jumps. The ABD model is implemented by depositing one atom on the surface at a time, leaving the next atom to wait while the adatom and the rest of surface atoms experience diffusional rearrangement to the extent allowed by the diffusion kinetics. The deposition rate controls the time between two arriving atoms (which corresponds to the normalized time to fill one monolayer of the film in a given simulation cell). The time increment between the arrivals of two atoms at the surface of the hexagonal lattice is thus

$$\Delta t = \frac{\sqrt{3}a}{2n J_\mathrm{r}} \tag{5}$$

where a is the lattice spacing, n the number of atoms in one monolayer, and J_r the instantaneous deposition rate as defined in Eq. (1). A faster deposition rate will thus reduce the time between two arriving atoms and thus the extent of surface relaxation allowed between arrivals.

Most of the deposition simulations of interest are conducted under conditions where thermally activated diffusion processes are active. Therefore, along with the deposition events, surface diffusion by all available surface atoms must be taken into account during a time period Δt. The classical dynamics of the jumping atom and its environment can be described by a classical transition state theory approach [35], wherein the motion of the atom is assumed to consist of independent, randomly oriented jumps between adjacent binding sites. In this case, each jump to a neighboring site will have a different probability determined by its activation energy, which in turn is assumed to depend on the change in coordination number during the jump. The probability of a jump is given by

$$p_i = \exp\left(-\frac{Q_i}{kT}\right) \tag{6}$$

where k is Boltzmann's constant, T is the deposition temperature, and Q_i the activation energy for a specific jump direction. Yang et al. calculated activation energies for different diffusion paths in a two-dimensional metallic Ni system using an embedded atom method [33]. Their results indicate that activation energies are higher to move to sites with smaller coordination numbers from those sites with larger coordination numbers, in qualitative agreement with the approach used by Müller [18]. In the absence of similar activation energies for YSZ, the values for Ni derived by Yang et al. [33] are adopted here to illustrate, albeit qualitatively, the relevant features of the problem.

The number of possible diffusional events in this study is finite and enumerable and thus it is beneficial to construct a table of the activation energies of all possible surface diffusion paths at the beginning of simulation. A KMC method is then utilized, wherein for each Monte Carlo step one event is selected among all possibilities and is then executed. This is in contrast to conventional MC, in which an event is chosen randomly and its acceptance is determined by a certain probability. The choice of an event in KMC is determined by the relative probability for each possible jump, i, described by Eq. (6). At each time (MC) step, one event denoted by m is chosen pseudo-randomly from all of the M events as given by

$$\frac{\sum_{i=0}^{m-1} p_i}{\sum_{i=0}^{M} p_i} < N_\mathrm{R} < \frac{\sum_{i=0}^{m} p_i}{\sum_{i=0}^{M} p_i} \tag{7}$$

where N_R is a random number, uniformly distributed between 0 and 1, and $p_0 = 0$ [34]. The system is examined only when a diffusion event occurs, in which case the clock will be advanced by time increment, δt, associated with each simulation step, as given by

$$\delta t = -\ln(N'_\mathrm{R})\left[\nu \sum_{i=1}^{M} p_i\right]^{-1} \tag{8}$$

where ν is the effective vibration frequency ($5\,\mathrm{ps}^{-1}$ in this study) and N'_R is a (new) random number, uniformly distributed between 0 and 1. The denominator in Eq. (8) represents the sum of the probabilities of all the possible events encountered during δt.

3. Results and discussion

Deposition conditions were systematically changed in order to isolate the effect of selected parameter on the development of film morphologies, as summarized in Table 1. To facilitate comparison with experiments performed in a related investigation, the normalized distance from the source was set as $d_0/r = 7.5$ for all simulations. Simulation cells with 120 and 200 atoms in width were used. Comparison of these cell sizes for the same set of conditions gave reasonably consistent results, so the smaller cell sizes were generally used to minimize computation time except where the larger cell was needed to provide a better representation of the morphology.

The total number of atoms deposited per simulation ranged from about 25,000 to 55,000, equivalent in most cases to only few revolutions. (Longer growth periods required increasing concomitantly the width of the cell and computation times beyond those practical in the present investigation.) Hence, the results should be taken as providing insight primarily on the early stages of growth. The primary focus will be on assessing the effects of changing conditions on the extent of void formation and the characteristics of the microstructure.

Because of the inherent limitations of the two-dimensional model (see Section 4), the associated activation energies and possibly the cell size, it was found that the relevant range of the homologous scale (T/T_M) over which porosity formation is predicted in the computations is significantly lower than that typical of the experiments ($\sim 0.43 \pm 0.03 T_M$). Since a temperature of $\sim 0.25 T_M$ yields a dense film under stationary deposition (for a typical deposition rate of ~ 1 μm/min), but porous under rotation, the temperature range of $0.2–0.3 T_M$ was selected for the simulations. The salient findings are described and discussed below.

3.1. Deposition on planar substrates

The effect of rotation on the morphology of the film is first examined in the absence of surface diffusion, i.e. when deposition takes place at very low homologous temperature ($T/T_M \rightarrow 0$). In consequence, the film is very porous as illustrated in Fig. 4(a). An inverse C-shaped morphology is readily evident in each layer, revealing the tendency of the growth to follow the changing direction of the incident vapor. The pattern is qualitatively consistent with experimental observations of the near interface layer in actual TBCs [36,37]. Features reminiscent of columnar growth are also evident in the simulation, but are all within a "single crystal", whereas in a real coating the columnar structure is defined first and foremost by the competitive growth of grains with favorable crystallographic orientations [38]. It is also noted in Fig. 4(a) that the film is not uniformly porous but the porosity appears to be preferentially accumulated in the regions of highest vapor incidence angle, i.e. near the "sunrise" and "sunset" conditions. This is confirmed by the histogram of Fig. 4(b), reflecting the number of atoms deposited per layer as a function of distance from the substrate. As much as 50% of the monolayer sites can be vacant near the points where the end of one revolution overlaps with the beginning of the next.

Table 1
Deposition conditions used in the simulation

Substrate temperature, T/T_M	0.20–0.30
Net deposition rate (μm/min)	0.5–1.0
Substrate rotation speed, ω (rpm)	10–40
Normalized distance from source, d_0/r	7.5
Vapor incidence angle, α	
Stationary (°)	0
Rotating (°)	$-90 \leq \theta \leq 90$
Width of the simulation cell (atoms)	120 or 200
Size of the simulation (atoms)	21000–56000

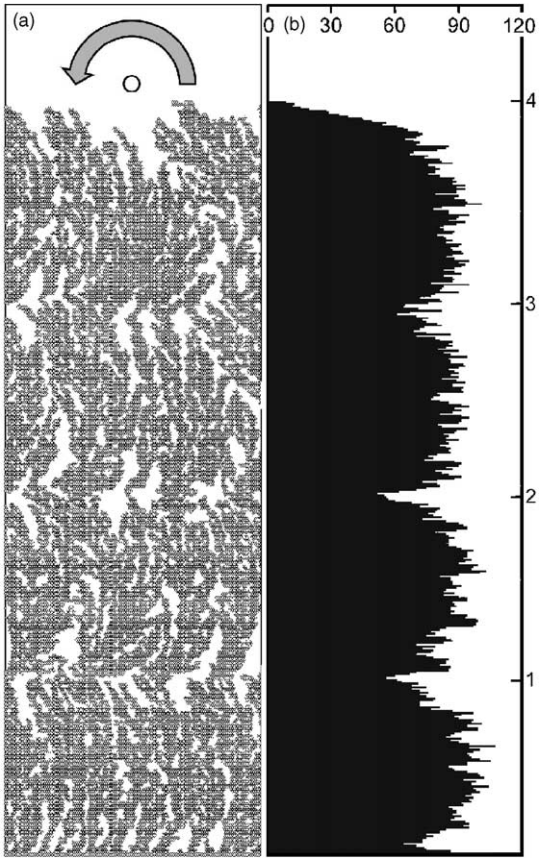

Fig. 4. Simulated film morphology resulting from growth under substrate rotation but without surface diffusion. The cell width was 120 atoms, the deposition rate was 1 μm/min and the rotation speed 20 rpm. (a) Inverted "C"-shape features resulting from a vapor source describing a counterclockwise "sunrise–sunset" pattern over a planar substrate. (b) Histogram showing the number of atoms deposited per layer corresponding to the morphology in (a). The scale on the right indicates the end of each successive revolution.

While the growth front is certainly not planar and, after the initial stage, deposition occurs on a multiplicity of planes in any given time increment, the influence of the rotation pattern is still evident on the distribution of porosity.

Incorporating limited surface diffusion ($T/T_M = 0.25$) produces a much denser film for comparable deposition and rotation rates, as illustrated in Fig. 5(a). Columnar features are now well developed albeit crystallographically indistinct, falling within the same two-dimensional "single crystal" as in the previous calculation. Voids appear in rows along the "column boundaries", corresponding to the valleys in the growth front. These are the points of highest shadowing when the more oblique components of the incident vapor interact with the morphology of the growth front. The periodicity of the voids is consistent on average with the thickness deposited per revolution, and their shape often reflects the inverted "C"-shape morphology discussed above (see also Figs. 6 and 9). It is also noted that the first layer contains no voids, revealing that a certain amount of roughness is needed to induce sufficient shadowing to overcome the effect of the surface diffusion in redistributing the deposited atoms. In contrast,

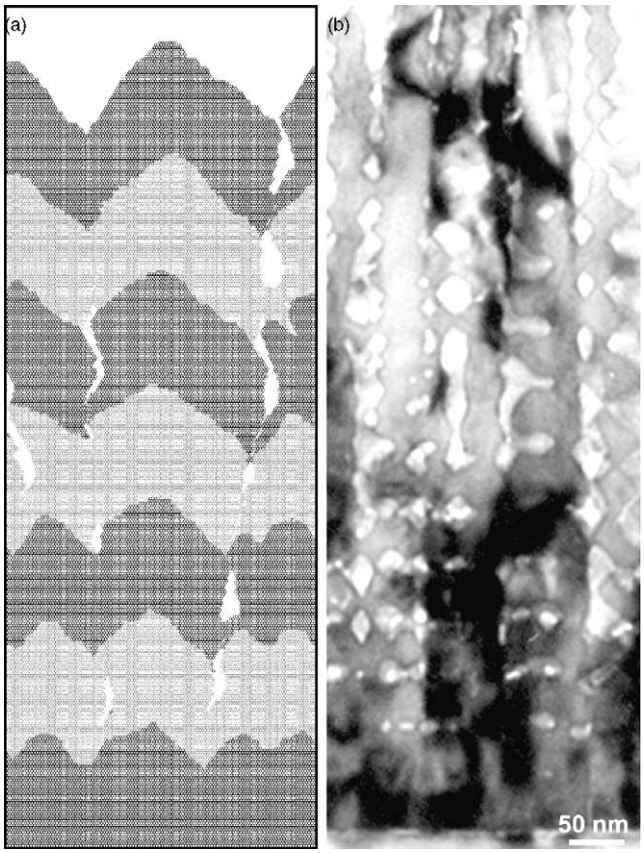

Fig. 5. Void formation under rotation in the presence of surface diffusion: (a) ABD model with the same cell size and deposition rate as in Fig. 4 but a rotation speed of 30 rpm and a temperature $T/T_M = 0.25$. The different shades of gray delineate the amount of material deposited in each revolution. (b) Periodic void formation between columns near the interface of a vapor-grown YSZ film and a planar sapphire substrate (courtesy of B. Raschkova and M. Rühle [39]). The periodicity of the voids (∼35 nm) is consistent with the amount of material deposited per revolution in the experiment. Note the absence of voids between the first and second layers.

voids emerge almost immediately in the absence of surface diffusion, as noted in Fig. 4(a).

The type of "pearl-string" porosity in Fig. 5(a) is experimentally observed at the boundaries of YSZ columns grown on a polished sapphire substrate, as illustrated in Fig. 5(b), as well as within larger columns that have undergone internal segmentation [13]. The columns in Fig. 5(b) are crystallographically distinct but with a common out-of-plane orientation due to the templating effect of the single-crystalline substrate [39]. The nanoscale voids have a spacing of ∼35 nm, consistent with the amount of material deposited in one revolution. As in the simulation, it is evident that voids do not start in the first layer but require the development of a critical amount of roughness at the growth front before shadowing predominates over surface diffusion. In this case, however, the roughness is crystallographic in nature since columns tend to grow with pointed tips even at this early stage [8,13]. In contrast, the origin of the roughness in the simulation is largely stochastic. The evolution of the

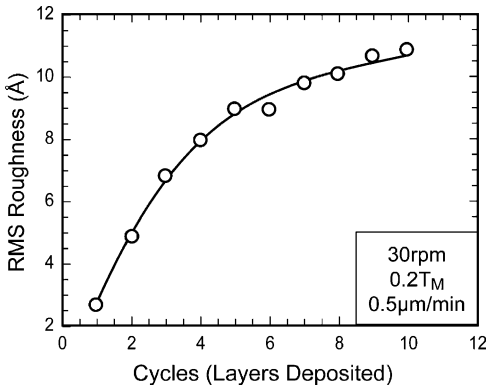

Fig. 6. Evolution of surface RMS roughness (Å) with increasing number of revolutions (layers deposited) for a simulated film grown at $0.2T_M$, 0.5 μm/min and 30 rpm.

RMS surface roughness for a longer simulation is illustrated in Fig. 6. Fig. 5(a) further shows that the "wavelength" of the surface roughness also increases during growth, giving the appearance of column widening reminiscent of real TBC microstructures. The effect, however, misses the dominant

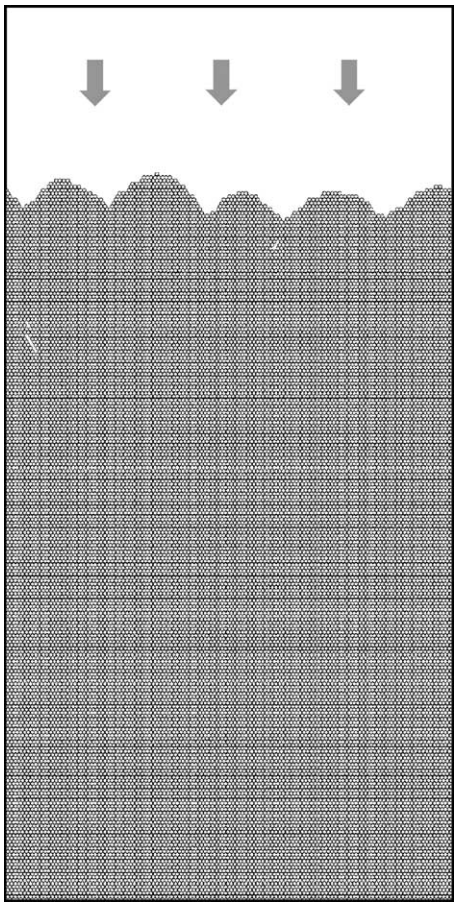

Fig. 7. Simulated morphology for a film grown on a stationary substrate with normal vapor incidence ($\alpha = \theta = 0°$). The deposition temperature and rate were $0.25T_M$ and 1 μm/min, respectively. The simulation cell width was 120 atoms.

crystallographic effects giving rise to evolutionary selection and the ensuing column widening in the real situation. It is also noted that in actual TBC coatings the "pearl-string" porosity is not typically observed at column boundaries, which instead are separated by continuous gaps. The source of these is discussed in Section 3.2.

Surface diffusion during "nighttime", i.e. when there is no concurrent deposition of atoms, appears not to contribute significantly to further densification of the film in these simulations. Comparison of film morphologies immediately after "sunset" and before "sunrise" for the next revolution did not show detectable differences, even though surface diffusion was allowed to proceed during this period at the same nominal temperature but with $J_r = 0$. The inference is that, for the conditions investigated, the surface can relax to a near-equilibrium state between two consecutive arrival events, i.e. $\delta t \ll \Delta t$ (Eqs. (5) and (8)). Hence, the deposition rate is never sufficiently high in these simulations to "bury" void structures that could undergo substantial reconfiguration during the "nighttime" period. Such scenarios, however, could evolve in principle if the combination of deposition rate and temperature were to translate into $\delta t \rightarrow \Delta t$. This would imply moving toward the transition between zones 1 and 2 in the Movchan and Demchishin structure map [7], but the situation is not particularly relevant for TBC deposition since adhesion in this temperature range is poor.

The critical effect of rotation is highlighted when comparing Figs. 5(a) and 7. The latter depicts simulated film growth on a stationary substrate and normal incidence, at the same conditions of temperature ($T/T_M = 0.25$) and deposition rate (1 μm/min) as in Fig. 5(a). The film in Fig. 7 is essentially dense but for the presence of a few minute pores. These pores are primarily the result of occasional "overhangs" which may develop due to the hexagonal lattice geometry and can induce shadowing even for vapor atoms impinging normal to the substrate. Similar phenomena are feasible in experimental film growth situations, although for TBCs the more likely source is the inherent variability in VIA associated with a "point source" moving over a finite width evaporating pool, as discussed elsewhere [8,40]. Nevertheless, the net effect of rotation may be summarized as enhancing shadowing and thus shifting the zones in the Movchan and Demchishin structure map [7] to higher temperatures.

The effect of temperature at constant rotation and deposition rates is illustrated in Fig. 8. The film becomes progressively dense with increasing temperature up to a point in which substrate diffusion completely predominates shadowing and eliminates the porosity. Two effects are worth

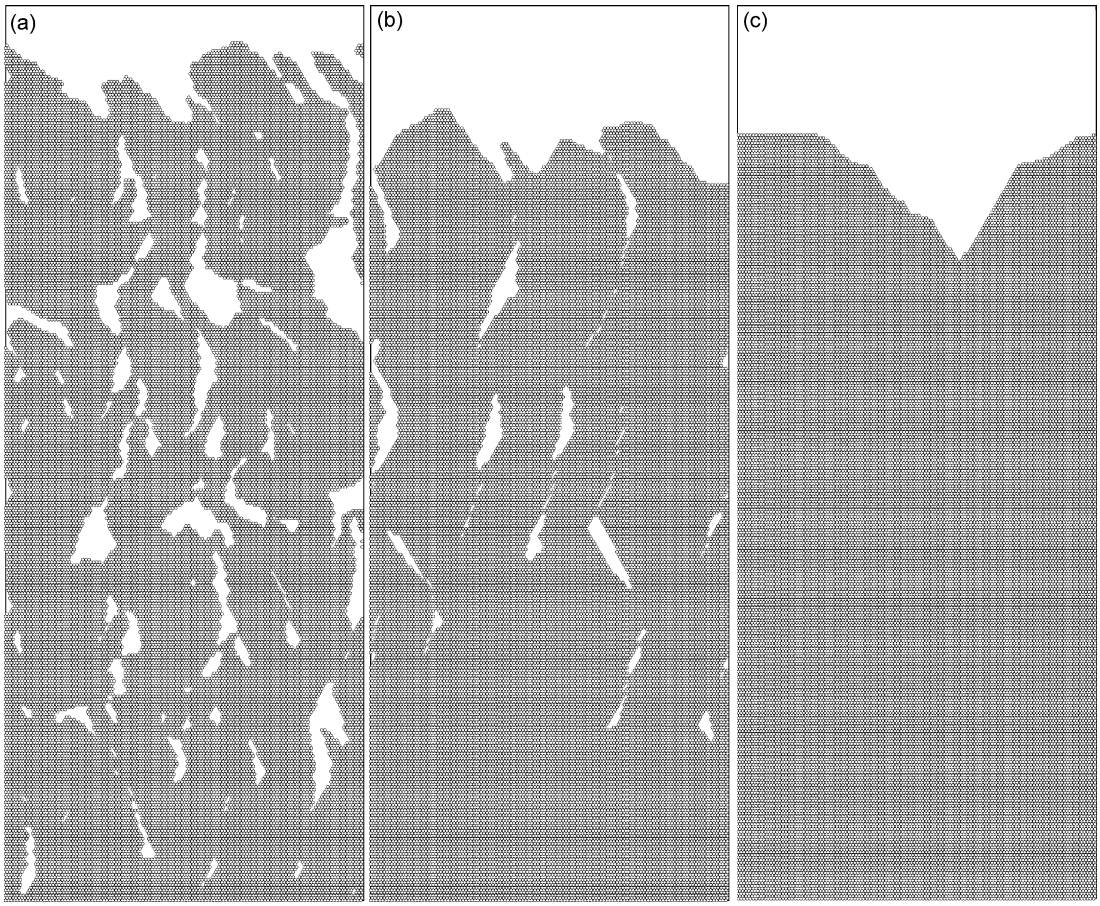

Fig. 8. Comparison of simulated morphologies for films grown at different substrate temperatures: (a) $0.20T_m$; (b) $0.25T_m$; (c) $0.30T_m$. The simulation cell was 120 atoms wide, the deposition rate 1 μm/min and the substrates rotated at 20 rpm.

noting. One is the rather dramatic effect of a seemingly modest increase in the deposition temperature (0.2–0.3T_M). This is partly the result of the limitations inherent in the two-dimensional model and the menu of possible jumps and activation energies assumed. The second effect arises from the limited cell size. A wider cell would allow longer simulations that could eventually result in porosity as the scale of the surface roughness continues to increase. These limitations notwithstanding, the basic physics of the interplay between rotation and surface diffusion is captured by this set of simulations.

The influence of rotation speed on film morphology for growth at a constant temperature (0.25T_M) and deposition rate (1 μm/min) is depicted in Fig. 9. Comparison is done at the same deposited thickness and thus the number of revolutions is different in each case. In general, the effects of rotation speed are less prominent than those of temperature. The simulated differences in pore content and surface roughness are modest at best. The void morphologies change from a distinct inverse "C" pattern at the lower deposition rate (10 rpm, Fig. 9(a)) to rows of elongated vertical voids at the higher rate (40 rpm, Fig. 9(d)). A similar loss of the "bent column" morphology has been reported in the literature for growth on sapphire substrates [37], but other significant changes in column width and shape that are not captured in the simulations are also reported with increasing rotation rate [41].

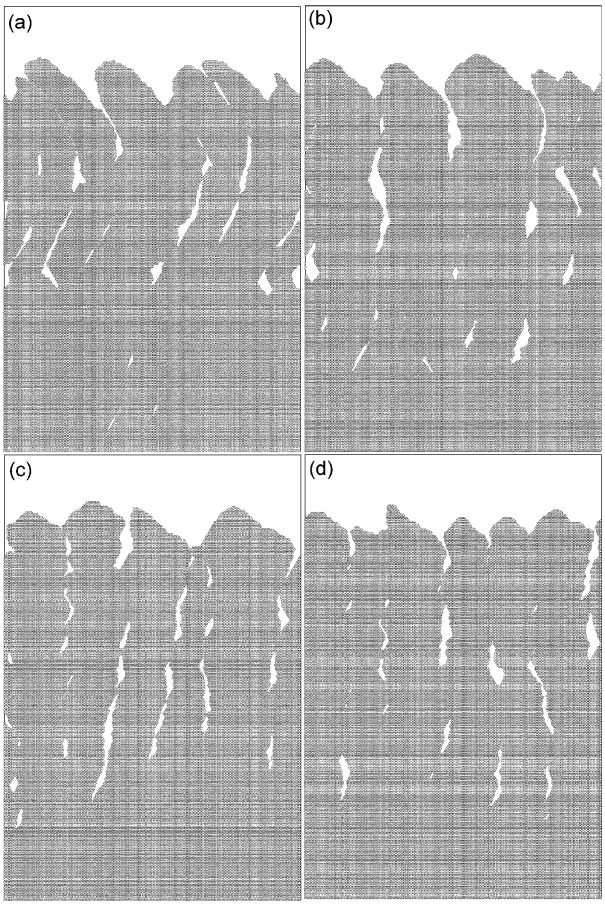

Fig. 9. Comparison of film morphologies for different rotation speeds at the same temperature (0.25T_M), deposition rate (1 μm/min), and total film thickness: (a) 10 rpm; (b) 20 rpm; (c) 30 rpm; (d) 40 rpm. The simulation cell width was 200 atoms.

In summary, the following trends emerge from these simulations on planar substrates. Substrate rotation at low temperatures shows a pronounced degree of void formation (Fig. 4), which persists at finite temperature (Fig. 5), though at sufficiently high temperatures the surface is completely dense (Fig. 8). Without rotation the surfaces are much denser (Fig. 7). The films show C-shaped columns at low rotation rate, with a transition to straight columns at higher rates, in qualitative agreement with experiment. Finally, there is a periodicity in the void formation consistent with the amount of material deposited per revolution, also in qualitative agreement with the experiments.

3.2. Deposition on non-planar substrates

Two situations are of interest in this section. The first one is the effect of a more realistic surface topography on which deposition may occur. Fig. 10(a) shows the near-interface region of a YSZ film deposited on a rotating substrate at a temperature of ∼0.4T_M and a rate of ∼1 μm/min. The metallic substrate was pre-oxidized prior to deposition forming a dense, polycrystalline α-Al_2O_3 layer on its surface. It is clearly evident that finite inter-columnar gaps initiate at the interface, typically at the "valleys" between neighboring Al_2O_3 grains. This illustrates two important points that are absent in Fig. 5. One is the presence of discrete gaps rather than rows of "pearl-string" pores at the column boundaries. This is primarily a result of a coarser initial structure with random grain orientations, rather than the finer grains with a common out-of-plane orientation induced by the polished sapphire substrate in Fig. 5(b). The second is the absence of a dense first layer, arguably because the need for developing an initial roughness is obviated by the presence of the polycrystalline Al_2O_3 layer.

To provide insight on the issues above, a simulation was undertaken wherein deposition occurred on an initial serrated profile, set by prescribing that the appropriate sites in the lattice were filled prior to the start of deposition. The initial profile and results of the simulated deposition are shown in Fig. 10(b). Pores nucleate within the first layer since shadowing sources are already present at the start of deposition. The pores are larger and more elongated than in Fig. 4(a), resembling the gap morphology in Fig. 10(a). However, the incipient gaps are partially closed after the second revolution, presumably because the scale of the problem is still much smaller than that in the experiment. There is also an interesting asymmetry in the initial deposition layer, which is thicker on the left-hand side of the valleys. This is the "morning" side in the "sunrise–sunset" pattern of vapor incidence, receiving vapor first while the right-hand side is completely shadowed by the saw-tooth peaks. In consequence, the "morning" side builds up first and enhances the shadowing effects on the

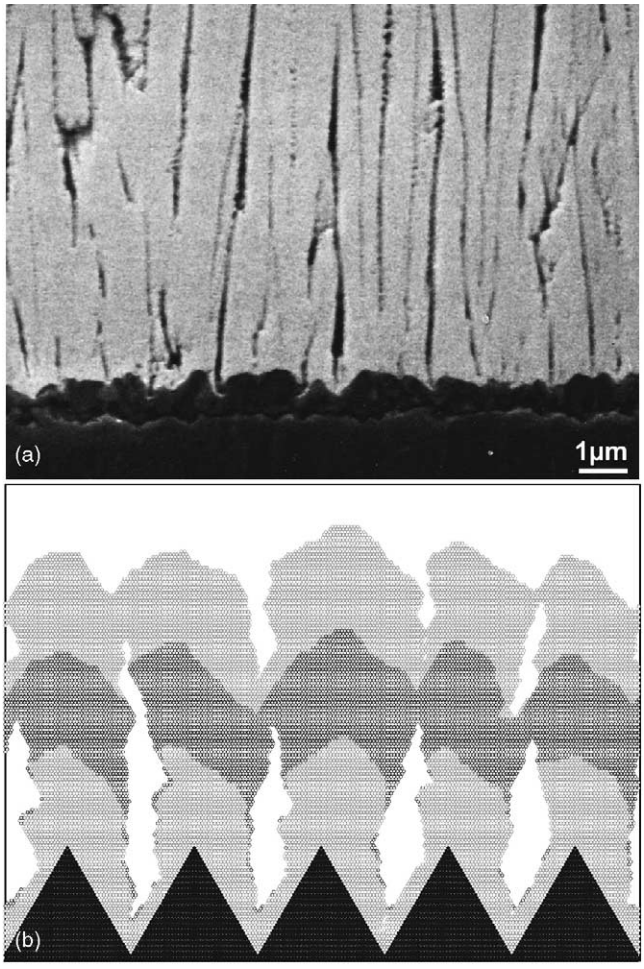

Fig. 10. Effect of initial surface roughness on film growth: (a) near-interface microstructure of a TBC deposited on a polished FeCrAlY substrate that was pre-oxidized to produce a thin layer of polycrystalline Al_2O_3 prior to deposition; (b) ABD model on an initially serrated surface (darker peaks) clearly showing the initiation of inter-columnar gaps at the valleys between alumina grains. Note that shadowing is enhanced on the right-hand sides of the valleys, because of deposition occurring earlier on the left-hand side. The cell was 200 atoms wide.

right-hand side of the valley when the latter receives flux during the "evening" part of the cycle.

The second situation of interest relates to the evolution of the intra-columnar "feathery" pores in Fig. 1, illustrated in greater detail in Fig. 11(a). These pores are thin and ribbon-like, oriented at an angle of ∼45° relative to the axis of the column. It has been proposed that these pores arise from shadowing by small crystallographic steps on the column tips [8,13]. To assess this hypothesis, a simulation was undertaken wherein the initial substrate profile included steps, as depicted in Fig. 11(b). (The actual steps in the experimental situation occur on inclined planes, but the problem is simplified here to facilitate the simulation.) The results clearly show voids propagating outward at an angle from each side of the initial steps, starting after some small amount of deposition but still within the first revolution. The net growth direction, however, is still normal to the base of the simulation cell. Asymmetry

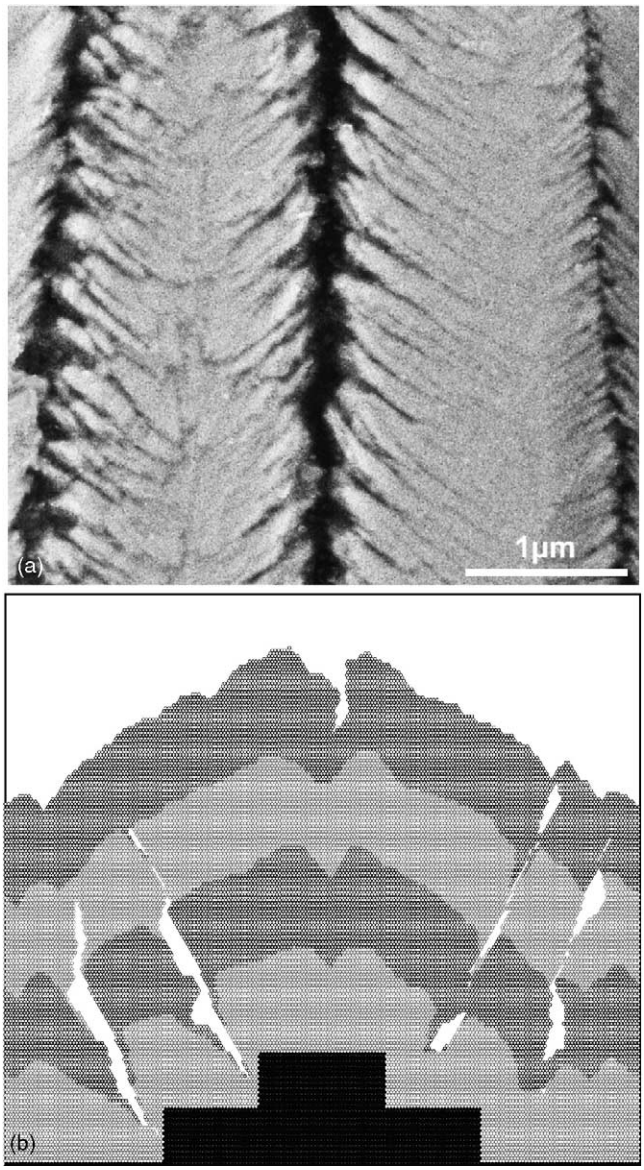

Fig. 11. Illustration of the role of surface steps in producing "feathery" porosity: (a) Polished cross-sectional view of YSZ TBC deposited on pre-oxidized FeCrAlY substrates showing thin ribbon-like pores at an angle to the column axis; (b) ABD model on a substrate containing initially three terraces at different levels. Note the role of the steps in initiating the inclined pores. The simulation cell was 200 atoms wide.

in the initiation of the voids is also evident in this simulation, with thicker build-up before pores start on the "morning" side of the steps than on their "evening" counterpart. Qualitative agreement with the experiment is deemed satisfactory, but refinement of the simulation is needed to study the mechanisms and ensuing morphologies in more detail.

4. Model limitations

While there is reasonable agreement between salient features of the vapor-grown TBC microstructures and the

present ABD/KMC simulations, it is evident that there is potential for substantial improvement in the model. An important limitation is imposed by the two-dimensional lattice, which inherently neglects relevant diffusion paths that exist in three dimensions. The number of nearest-neighbors interacting with a surface atom during a diffusion event is larger in a 3D model, suggesting that the corresponding activation energies and thus the required T/T_M to activate diffusion are both higher than in 2D. Jumps over a single atom are the norm in a 2D model, but much less likely in 3D where the atom may follow a path along valleys on the surface, always in contact with at least two atoms. Conversely, because one-neighbor sites are always unstable in this model, some potential jumps involving diffusion at surface steps [42] may be comparatively less likely than in a 3D approach.

A second important limitation is the absence of crystallographic influence in the film growth, which is well known to occur in the real deposition process. This precludes the incorporation of evolutionary selection mechanisms [38] that are responsible for texture development and the concomitant change in the scale of the columnar microstructure with increasing thickness. It is thus important to extend this model with a microstructural-scale simulation, in which the inherent texture information is included and the competition between growth directions is described with parameters determined by the related experiments [20,21]. This latter approach would in turn provide a connection between different length scales of simulation to better understand the experimental observations.

The third important limitation relates to the significant differences that may occur between deposition of metallic atoms and associated activation energies [33] and the deposition of multiple species on a surface where bonding is ionic (arguably with some element of covalency) as it occurs in YSZ. The Ni parameters were selected for the obvious reason that there are no equivalent values for YSZ, but also for computational reasons since simulation of ionic systems would involve long-range interactions that greatly increase the computing time. There are also a number of concerns regarding the accuracy of calculated activation energies for diffusion in ionic materials. These pertain to the relative inaccuracy of the interatomic potentials near a surface [43] as well as contributions from a space charge region associated with the surface [44]. While these limitations are important, the present simulations do reflect the basic physics of some of the phenomena of interest, helping elucidate the role of substrate rotation and its interplay with the deposition temperature.

5. Conclusion

The present model combines atomic ballistic deposition (ABD) with a kinetic Monte Carlo (KMC) algorithm for surface diffusion and a geometric algorithm to describe the "sunrise–sunset" pattern of vapor incidence peculiar to deposition of thermal barrier coatings. The model was successfully implemented and the resulting simulations provided insight into the effect of substrate rotation and the ensuing shadowing phenomena on film evolution. The simulations were generally consistent with experimental observations on the microstructure of YSZ TBCs, especially those grown on planar substrates.

The simulations highlighted the critical role of surface rotation on the evolution of both inter-columnar and intra-columnar forms of porosity. Pores arise from the interplay of surface topography with the oblique elements of the vapor flux during the rotation cycle. This presumes a certain amount of surface roughness, which could already be present in the substrate or arise as a result of stochastic deposition of atoms in the case of the simulation, or from the crystallographic nature of the column tips that evolve in the real coatings. Periodicities in the void structure arise either from the amount of material deposited per revolution ("pearl-string" pores), or from the scale of the features at the column tips ("feathery" pores). It is also found that temperature (and by extension deposition rate) has a much stronger effect on the content of porosity than the rotation rate, whose effects are reflected primarily in the pore morphology.

Significant opportunities exist for further improvement of the model with attendant benefits to the understanding of the experiments. Notably, the simulation could be extended to other length scales to incorporate the effects of texture development, and also to a three-dimensional lattice to provide a more realistic representation of surface diffusion.

Acknowledgments

This work was supported by Collaborative UC/Los Alamos Research (CULAR) Program. Additional support for S.G. Terry was provided through the Office of Naval Research under contract N00014-99-1-0471, monitored by Dr. S.G. Fishman. The work of R. LeSar was performed under the auspices of the United States Department of Energy (US DOE under contract W-7405-ENG-36) and was supported in part by the Division of Materials Science of the Office of Basic Energy Sciences of the Office of Science of the US DOE. The authors are grateful to Drs. J.Y. Yang and B. Raschkova, and to Prof. M. Rühle, for making available images to illustrate the modeling results in Figs. 1 and 5.

References

[1] M.J. Stiger, N.M. Yanar, M.G. Topping, F.S. Pettit, G.H. Meier, Zeitschrift Metallk. 90 (1999) 1069–1078.
[2] W. Beele, G. Marijnissen, A.H.F. van Lieshout, Surf. Coat. Technol. 120–121 (1999) 61–67.
[3] T.E. Strangman, Thin Solid Films 127 (1985) 93–105.
[4] D.H. Boone, T.E. Strangman, L.W. Wilson, J. Vac. Sci. Technol. 11 (1974) 641–646.

[5] H.J. Leamy, G.H. Gilmer, A.G. Dirks, The microstructure of vapor deposited thin films, in: E. Kaldis (Ed.), Current Topics in Materials Science, vol. 6, North-Holland, 1980, pp. 308–344.
[6] C. Leyens, U. Schulz, B.A. Pint, I.G. Wright, Surf. Coat. Technol. 120–121 (1999) 68–76.
[7] B.A. Movchan, A.V. Demchishin, Fizika Metallov i Metallovedenie 28 (1969) 83–90.
[8] S.G. Terry, Evolution of microstructure during the growth of thermal barrier coatings by electron-beam physical vapor deposition, Doctoral Dissertation in Materials, University of California, Santa Barbara, CA, 2001.
[9] T.J. Lu, C.G. Levi, H.N.G. Wadley, A.G. Evans, J. Am. Ceram. Soc. 84 (2001) 2937–2946.
[10] R. Subramanian, Thermal barrier coating having high phase stability, U.S. Patent 6,258,467 (2001).
[11] D. Zhu, R.A. Miller, Ceram. Eng. Sci. Proc. 23 (2002) 457–468.
[12] D. Zhu, Y.L. Chen, R.A. Miller, Ceram. Eng. Sci. Proc. 24 (2003) 525–534.
[13] S.G. Terry, C.G. Levi, Metall. Mater. Trans., submitted for publication.
[14] F.F. Abraham, G.M. White, J. Appl. Phys. 41 (1970) 1841–1849.
[15] D.J. Henderson, M.H. Brodsky, P. Chaudhari, Appl. Phys. Lett. 2 (1974) 641–643.
[16] S. Kim, D.J. Henderson, P. Chaudhari, Thin Solid Films 47 (1977) 155–158.
[17] R.A. Outlaw, J.H. Heinbockel, Thin Solid Films 108 (1983) 79–86.
[18] K.H. Müller, J. Appl. Phys. 58 (1985) 2573–2576.
[19] J.S. Gau, B. Liao, Thin Solid Films 176 (1989) 309–321.
[20] D.J. Srolovitz, D.S. Dandy, J.E. Butler, C.C. Battaile, F. Paritosh, J. Min. Met. Mater. Soc. 49 (1997) 42–47.
[21] F. Paritosh, D.J. Srolovitz, C.C. Battaile, X. Li, J.E. Butler, Acta Mater. 47 (1999) 2269–2281.
[22] H.C. Kang, W.H. Weinberg, J. Chem. Phys. 90 (1989) 2824– 2828.
[23] J. Dawnkaski, D. Srivastava, B.J. Garrison, Chem. Phys. Lett. 232 (1995) 524–530.
[24] X.W. Zhou, H.N.G. Wadley, J. Appl. Phys. 87 (2000) 557–563.
[25] A.B. Bortz, M.H. Kalos, J.L. Lebowitz, J. Comput. Phys. 17 (1975) 10–18.
[26] A.F. Voter, Phys. Rev. B 34 (1986) 6819–6829.
[27] C.C. Battaile, D.J. Srolovitz, J.E. Butler, J. Appl. Phys. 82 (1997) 6293–6300.
[28] H. Jeong, B. Kahng, S. Lee, C.Y. Kwak, A.L. Barabási, J.K. Furdyna, Phys. Rev. E 65 (2001) 031602.
[29] H.N.G. Wadley, X.W. Zhou, R.N. Johnson, M. Neurock, Prog. Mater. Res. 46 (2001) 329–377.
[30] U. Schulz, S.G. Terry, C.G. Levi, Mater. Sci. Eng. A 360 (2003) 319–329.
[31] S. Schiller, U. Heisig, S. Panzer, Electron Beam Technology, Wiley, New York, 1982.
[32] A.N. Belov, G.A. Semenov, Russ. J. Phys. Chem. 59 (1985) 342–344.
[33] Y.G. Yang, R.A. Johnson, H.N.G. Wadley, Acta Mater. 45 (1997) 1455–1468.
[34] C.C. Battaile, D.J. Srolovitz, Annu. Rev. Mater. Res. 32 (2002) 297–320.
[35] A.F. Voter, J.D. Doll, J. Chem. Phys. 80 (1984) 5832–5838.
[36] D.V. Rigney, R. Viguie, D.J. Wortman, PVD thermal barrier coating applications and process development for aircraft engines, in: W.J. Brindley (Ed.), Thermal Barrier Coating Workshop, Conference Publication 3312, NASA, Cleveland, OH, 1995, pp. 135–149.
[37] U. Schulz, M. Schmücker, Mater. Sci. Eng. A 276 (2000) 1–8.
[38] A. Van der Drift, Evolutionary Selection: A Principle Governing Growth Orientation in Vapour-deposited Layers, Philips Research Report No. 22, 1967, pp. 267–288.
[39] B. Raschkova, Microstructural characterization of yttria-stabilized zirconia thermal barrier coatings grown on sapphire substrates, Doctoral Dissertation in Materials Science, Universitaet Stuttgart, Stuttgart, Germany, 2004, 126 pp.
[40] S.G. Terry, J.R. Litty, C.G. Levi, Evolution of porosity and texture in thermal barrier coatings grown by EB-PVD, in: J.M. Hampikian, N.B. Dahotre (Eds.), Elevated Temperature Coatings: Science and Technology III, The Minerals, Metals and Materials Society, Warrendale, PA, 1999, pp. 13–25.
[41] W.A. Kaysser, M. Peters, K. Fritscher, U. Schulz, Processing, characterisation and testing of EB-PVD thermal barrier coatings, in: AGARD Structures and Materials Panel Meeting on Thermal Barrier Coatings, AGARD R-823, AGARD (Advisory Group for Aerospace Research and Development), Aalborg, Denmark, 1998, pp. 9.1–9.11.
[42] R.L. Schwoebel, E.J. Shipsey, J. Appl. Phys. 37 (1966) 3682–3686.
[43] D. Wolf, J. Am. Ceram. Soc. 67 (1984) 1–13.
[44] K.L. Kliewer, J.S. Koehler, Phys. Rev. 140 (1965) 1226–1239.